

University of Texas Rio Grande Valley

ScholarWorks @ UTRGV

Health & Biomedical Sciences Faculty
Publications and Presentations

College of Health Professions

6-1-2022

Effect of drug-to-lipid ratio on nanodisc-based tenofovir drug delivery to the brain for HIV-1 infection

Caroline R. Garcia

The University of Texas Rio Grande Valley

Armin T. Rad

Farnoosh Saeedinejad

Arvind Manojkumar

The University of Texas Rio Grande Valley

Deepa Roy

The University of Texas Rio Grande Valley

See next page for additional authors

Follow this and additional works at: https://scholarworks.utrgv.edu/hbs_fac



Part of the [Medicine and Health Sciences Commons](#)

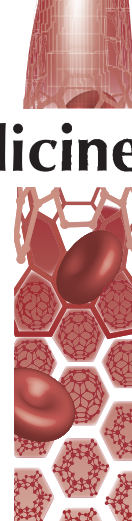
Recommended Citation

Garcia, C. R., Rad, A. T., Saeedinejad, F., Manojkumar, A., Roy, D., Rodrigo, H., Chew, S. A., Rahman, Z., Nieh, M. P., & Roy, U. (2022). Effect of drug-to-lipid ratio on nanodisc-based tenofovir drug delivery to the brain for HIV-1 infection. *Nanomedicine (London, England)*, 17(13), 959–978. <https://doi.org/10.2217/nnm-2022-0043>








This Article is brought to you for free and open access by the College of Health Professions at ScholarWorks @ UTRGV. It has been accepted for inclusion in Health & Biomedical Sciences Faculty Publications and Presentations by an authorized administrator of ScholarWorks @ UTRGV. For more information, please contact justin.white@utrgv.edu, william.flores01@utrgv.edu.

Authors

Caroline R. Garcia, Armin T. Rad, Farnoosh Saeedinejad, Arvind Manojkumar, Deepa Roy, Hansapani Rodrigo, Sue Anne Chew, Ziyaur Rahman, Mu-Ping Nieh, and Upal Roy



Effect of drug-to-lipid ratio on nanodisc-based tenofovir drug delivery to the brain for HIV-1 infection

Caroline R Garcia^{‡,1} , Armin T Rad^{‡,2,3,4} , Farnoosh Saeedinejad^{2,3} , Arvind Manojkumar¹, Deepa Roy¹, Hansapani Rodrigo⁵, Sue Anne Chew¹ , Ziyaur Rahman⁶ , Mu-Ping Nieh^{2,3}  & Upal Roy^{*,1} 

¹Department of Health & Biomedical Sciences, University of Texas Rio Grande Valley, Brownsville, TX, USA

²Department of Biomedical Engineering, University of Connecticut, Storrs, CT 06269, USA

³Polymer Program, Institute of Materials Sciences, University of Connecticut, Storrs, CT 06269, USA

⁴Encapsulate, University of Connecticut Technology Incubation Program, Farmington, CT 06032, USA

⁵Department of Mathematical & Statistical Sciences, University of Texas Rio Grande Valley, Edinburg, TX, USA

⁶Irma Lerma Rangel College of Pharmacy, Texas A&M Health Science Center, Texas A&M University, College Station, TX 77843, USA

*Author for correspondence: upal.roy@utrgv.edu

[‡]Authors contributed equally

Background: Combination antiretroviral therapy has significantly advanced HIV-1 infection treatment. However, HIV-1 remains persistent in the brain; the inaccessibility of the blood–brain barrier allows for persistent HIV-1 infections and neuroinflammation. Nanotechnology-based drug carriers such as nanodiscoidal bicelles can provide a solution to combat this challenge. **Methods:** This study investigated the safety and extended release of a combination antiretroviral therapy drug (tenofovir)-loaded nanodiscs for HIV-1 treatment in the brain both *in vitro* and *in vivo*. **Result:** The nanodiscs entrapped the drug in their interior hydrophobic core and released the payload at the desired location and in a controlled release pattern. The study also included a comparative pharmacokinetic analysis of nanodisc formulations in *in vitro* and *in vivo* models. **Conclusion:** The study provides potential applications of nanodiscs for HIV-1 therapy development.

First draft submitted: 1 March 2021; Accepted for publication: 6 May 2022; Published online: 1 June 2022

Keywords: blood–brain barrier • drug delivery • HIV-1 • nanodisc • nanomedicine

Over the past decades, HIV-1 treatment has been revolutionized by significant progress in therapeutic options such as combination antiretroviral therapy (cART) that control HIV-1 infection [1]. Through the development of cART, HIV-1 infection has been transformed from a deadly disease to a relatively manageable chronic illness. The cART helps reduce the morbidity caused by reducing the viral load in the plasma of people with HIV-1 [1,2]. Considering the rapid improvement of disease pathology through cART, the Joint United Nations Programme on HIV/AIDS (UNAIDS) developed a 90–90–90 treatment target in 2013 to help end this epidemic by 2020 [3]. Unfortunately, UNAIDS has fallen short of its 2020 goal, and developing an effective cART drug-delivery system remains a challenge [4]. The main reason is that HIV-1 is found in latent reservoirs such as the CNS, where cART drugs have restricted access due to lower permeability across the blood–brain barrier (BBB) [2,5].

Additionally, patients often struggle to follow their medication schedule due to significant side effects, which result in suboptimal therapeutic drug levels within the body, the rapid rebound of viral replication, mutations and treatment failure [1]. An increasing amount of evidence also shows that long-term use of cART is associated with neurological toxicity which may include peripheral neuropathy or neurocognitive deficits [5]. The BBB's inaccessibility allows for persistent HIV-1 infections and HIV-associated neurocognitive disorder (HAND), which is the most common manifestation of HIV-1 pathogenesis within the CNS [5]. While cART regimens have effectively reduced peripheral viral load, the prevalence of different forms of HAND, such as asymptomatic neurocognitive impairment, mild neurocognitive disorder and HIV-associated dementia, increases as HIV-1 patients age [5,6]. Thus optimizing the drug dosing that can reach viral reservoirs with minimum side effects for the patients is the current challenge.

In the last decades, nanotechnology has been extensively used in the field of medicine to develop the next generation of targeted therapies for many diseases, a field that is often referred to as nanomedicine or precision medicine [7]. Drugs with very low solubility, such as most anti-HIV drugs, present various challenges for pharmaceutical optimization, including a suboptimal concentration of drug in the tissues, less diffusion capacity and a requirement for frequent dosing or larger quantities for intravenous intake; however, nanomedicine represents an excellent strategy to overcome the limitations of conventional drug-delivery systems [7,8]. Several properties determine successful nanoparticle (NP)-mediated drug delivery, including biocompatibility, circulation shelf life and high drug-loading capacity. In this regard, several nanocarriers, such as solid lipid NPs [9], liposomes [10], polymeric micelles [11], dendrimers [12], oil bodies [13], aptamers [14] and nanoporous lipid bilayers [15], have been characterized for their potential for *in vivo* drug delivery [11,16].

A successful drug delivery also depends on the shape and size of the particle, which are crucial for cellular uptake [17,18]. Several studies have demonstrated the morphology of the NP determining the efficacy of the drug delivery [19,20]. A recent study has shown that self-assembled micelles have much enhanced cellular uptake compared with vesicles with the same or similar composition [21–24]. NPs with a diameter ranging from 20 to 100 nm resulted in optimal accumulation in tumors, with an enhanced permeability and retention effect [25,26]; different enhanced permeability and retention effects have been observed in nanorods in terms of their *in vivo* hydrodynamic behaviors, circulation and extravasation into the tumor [27,28]. NPs that are smaller than 100 nm, such as liposomes, have some advantages over rod-shaped particles [19,29].

Liposomes are one of the most widely used delivery vehicles for carrying agents. Liposomes have several advantages over other nanodelivery systems by being less toxic and having a high therapeutic index [30,31]. They have advantages such as protecting drugs or other therapeutic agents from degradation, targeting the site of action through ligand–peptide or –antibody conjugation, and have been noted to have little toxicity or side effects [32]. Nanodiscoidal-shaped bicelles or nanodiscs (NDs) share a similar chemical composition with liposomes but have not been studied extensively. NDs can be generated with control of lipid content and particle size due to their low polydispersity. They have the property of spontaneously forming discoidal bicelles that can entrap hydrophobic drugs; they consist of short- and long-chain lipids and are around 30 nm in diameter and 5 nm in thickness [33,34]. NDs are stable soluble membrane mimetics, a property that allows for further improvements, such as tagging to scaffold proteins; thus NDs provide a suitable model for studying membrane proteins [35,36]. This formulation allows large-scale production. During the manufacturing process, a disc-to-vesicle structural transition process occurs as the long-chain lipid molecule goes through from the low-temperature gel (order) to high-temperature L_a (liquid disorder) phase. Even though NDs and nanovesicles present similar dimensions, structurally they are not reversible at a lower temperature and remain intact in a uniform shape and size [34,37,38].

In the present study, nanodiscoidal bicelles offer an optimal structure for lipid-based drug delivery to assist in entrapping hydrophobic molecules until the body has metabolized them. Previous studies have demonstrated that ND bicelles can serve as nanocarriers to deliver hydrophobic molecules to cancerous cells [39]. The cellular uptake of the bicelles was approximately five- to ten-times greater than that of spherical vesicles or liposomes with an identical chemical composition [35,39]. In the present study we have expanded our previous observation of NDs with one of the anti-HIV drugs currently recommended by WHO for HIV-1 infection treatment [40]. An ND formulation was developed and characterized using this cART drug, tenofovir (TFV; a nucleoside reverse transcriptase inhibitor). This study aims to develop an ND formulation of TFV (ND–TFV) to perform extended drug release for effective long-term inhibition of HIV-1.

Materials & methods

Materials

All solvents (methanol, ethanol, chloroform and toluene) were purchased from Sigma-Aldrich (MO, USA) and filtered with a 0.2- μ m filter before use. Zwitterionic long-chain dipalmitoyl phosphatidylcholine (DPPC; di-16:0, catalog #850355P), charged long-chain dipalmitoyl phosphatidylglycerol (DPPG; di-16:0, catalog # 840455), zwitterionic short-chain dihexanoyl phosphatidylcholine (DHPC; di-6:0, catalog # 850305C) and PEG2000-conjugated distearoyl phosphoethanolamine (DSPE-PEG2000; catalog # 880120) were purchased from Avanti Polar Lipids (AL, USA) and used without further purification. Dulbecco's phosphate-buffered saline (PBS) and fetal bovine serum (FBS) were purchased from Life Technologies (NY, USA). Cremophor EL (Crem) was purchased from Sigma-Aldrich. Human embryonic microglial clone 3 cells (HMC-3) and human neuroblastoma cells (SH-SY5Y) were purchased from American Type Culture Collection (ATCC; VA, USA). The transformed cell lines retain

the properties. Primary human brain microvascular endothelial cells (HBMVECs; Catalog # 1000) and human astrocytes (HAs; catalog #: 1870) were obtained from ScienCell Research Laboratories (CA, USA) and cultured with their provided specialty mediums. Cells were cultured with Eagle's Minimum Essential Medium (Catalog # 30-2003, ATCC) supplemented with FBS to a final concentration of 10%, Dulbecco's PBS 1× (catalog # 30-2200, ATCC), TFV (catalog # PHR1592, Sigma-Aldrich), CellTiter 96[®] Aqueous One Solution Cell Proliferation Assay (Catalog # G3582; Promega, WI, USA), BioTek Synergy HT multi-mode microplate reader (BioTek, VT, USA) and Pur-A-Lyzer[™] Maxi 6000 Dialysis Kit (Sigma-Aldrich) were purchased from the listed vendors.

Methods

Preparation of NDs

Nanodiscoidal bicelles were prepared via self-assembly, as previously described [36,41]. For TVF-loaded NDs, the desired ratios of lipids and TVF were homogenized in a solution of chloroform, methanol and DMSO (13:7:5). The organic solvents were dried through a nitrogen purge at 58°C and desiccated at room temperature overnight in a vacuum oven to remove any residual solvent. The dried lipid or lipid and drug mixtures were homogeneously hydrated with filtered deionized water to 10 wt% through temperature cycling and vortexing. The experiments were performed with the samples diluted to 1.0 or 0.1 wt% depending on the experimental requirements [42]. The formulation of the samples with the lipid and drug concentrations is summarized in **Supplementary Table 1**. The drug-loaded NDs were further centrifuged at 5000 r.p.m. for 10 mins to separate unencapsulated and large drug/lipid complexes. The lipid composition of the bicelle remains constant throughout the samples (DPPC:DHPC:DPPG:DSPE-PEG2000 = 66.6:25.1:3.8:3.8) and drug-to-lipid molar ratios studied were 1:20 and 1:4. Drug-to-lipid ratios are considered theoretical and based on how much lipid and drug is being used in the whole solution, which can be calculated to know the amount of lipid and drug to add [43,44].

Structural characterization

Computational molecular modeling & calculations

Molecular simulation studies were carried out to understand the interactions between TFV and lipid molecules. The molecular lipophilic surface potential (MLSP) and molecular electrostatic potential (MEP) of TFV were calculated using VEGA-ZZ 3.2.0 software (Drug Design Laboratory, Milan, Italy). MEP is used to depict the 3D charge distributions of a molecule, and MLSP simulates the combined lipophilicity of a molecule's fragments at given point in space using the Molinspiration Property Calculation Service molecular [45], which is based on the Gasteiger–Hückel charges of the atoms [46,47]. The color ramp for the MLSP ranges from violet/blue (higher lipophilicity or greater lipophilicity potential) to red (lower lipophilicity or lower lipophilicity potential).

Small- & wide-angle x-ray scattering

Small- & wide-angle x-ray scattering (SAXS/WAXS) was used to analyze the structure of the bicelles. Before measurements, samples were ultrasonicated in a water bath for 30 min and vortexed for 10 min. Samples were tested at lipid concentrations of 10 mg/ml. SAXS/WAXS measurements were conducted at 16ID-LiX Beamline at National Synchrotron Light Source II, located at the Brookhaven National Laboratory (Upton, NY, USA), using the standard flow-cell-based solution scattering setup with x-ray energy of 13.5 keV. The SAXS/WAXS intensity is expressed as a function of the scattering vector, q ($q \equiv \frac{4\pi}{\lambda} \sin \frac{\theta}{2}$, where θ is the scattering angle) varies from 0.005 to 2.5 Å⁻¹ [48]. Radial averaging and q -conversion of data were performed using the standard software [49] by merging the data collected from all three detectors in the measurements. Transmission correction and background subtraction were performed to minimize the hydrogen bond's intensity from water at ~2.0 Å⁻¹.

Dynamic light scattering

The size and population distribution of the nanocarriers were determined using an ALV/CGS-8F/4 (ALV compact goniometer system, Malvern Instruments Ltd. Worcestershire, UK) instrument equipped with a 632.8-nm laser beam. The samples were dissolved in ultrapure distilled filtered water to 0.1 wt% and vortexed before each measurement. Results were an average of ten measurements.

ζ-Potential

The ζ-potential was measured within 30 min of sample preparation. The measurements were recorded in triplicate, and the averages of the results were used for data representation purposes using a 90Plus Particle Size Analyzer (Brookhaven Instruments Corp., NY, USA).

Cell viability assay of NDs

Cytotoxicity of NDs was determined via a 3-(4,5-dimethylthiazol-2-yl)-5-(3-carboxymethoxyphenyl)-2-(4-sulfophenyl)-2H-tetrazolium (MTS) assay on HMC-3 and SH-SY5Y cells. Cells were cultured in 96-well black-bottomed plates at 50,000 cells per well and incubated at 37°C in a humidified 5% CO₂ atmosphere for 24 h to allow for 70% confluency [50]. After 24 h, cells were treated with various empty ND concentrations (0.01–0.1 mg/ml) for 72 h. Unformulated TFV (Sigma-Aldrich) (also called free drug or FD-TFV) was also measured in similar conditions simultaneously. Untreated cells, incubated with fresh growth medium only, were considered as controls. After incubation, cells were washed and incubated with 100 µl of fresh cell medium. Cells were incubated with 20 µl of MTS reagent (CellTiter 96® AQueous One Solution; Promega) per the manufacturer's instructions, along with 100 µl of cell medium for 1 h at 37°C in a humidified 5% CO₂ atmosphere. After incubation, absorbance readings at 490 nm were taken using the BioTek Synergy HT multi-mode microplate reader hourly for 4 h, for a total of five measurements. The MTS assay was performed, and the optical density of the culture supernatant was measured at 490 nm. The net absorbance (sample absorbance – absorbance of blank) was taken as an index of cell viability of the treated and untreated cells. All measurements were taken as three independently replicated experiments of six values each. Cell viability was calculated using the following equation: $\frac{\text{Sample}}{\text{Control}} \times 100\%$.

Reactive oxygen species assay

Reactive oxygen species (ROS) productions in HMC-3 and SH-SY5Y cells following ND treatment were detected using the dichlorofluorescein diacetate assay (Molecular Probes, OR, USA). Cells were cultured in 96-well black-bottomed plates at 100,000 cells per well and incubated at 37°C in a humidified 5% CO₂ atmosphere for 24 h to allow for 70% confluency. The following day, the cell medium was taken out from each well and replenished with 100 µl of PBS + 1% FBS. Negative control cells were treated with antioxidant catalase, and the plate was incubated for 2 h. After incubation, the medium was taken out and replenished with 100 µM dichlorofluorescein diacetate (made with PBS + 1% FBS) to each well and incubated for 1 h. Following incubation, cells were treated with various concentrations (0.01–0.1 mg/ml of TFV) of the 1:4 and 1:20 ND-TFV and incubated for 2 h. A study of FD-TFV was also measured simultaneously. Cells with no drug (untreated) were incubated with a growth medium and used as control. Further cells were also treated with H₂O₂ (50 µM) for positive controls. After 2 h, the first reading of cell ROS production was read in the BioTek Synergy HT multi-mode microplate reader and then taken every hour for the following 18 h (excitation, 485 nm; emission, 528 nm) [50]. All measurements were taken as three independently replicated experiments of five values each.

In vitro sustained drug release assay of ND-TFV

The drug release kinetics of the ND-based drug delivery were determined in PBS using equilibrium dialysis. A 50-µl solution of the 5 mg/ml 1:4 and 1:20 ND-TFV formulated TFV, along with 1 ml of PBS, was placed into a dialysis bag (Pur-A-Lyzer™ Maxi 6000 Dialysis Kit, Sigma-Aldrich; molecular cutoff 6–8 kDa), sealed and put into a 50-ml conical tube filled with 20 ml of PBS with 0.1% Tween® 20 aqueous solution. The tube was then placed on a shaker at 37°C and rotated at 150 r.p.m. At scheduled intervals (0, 5, 10, 15 and 30 min; 1, 2, 4 and 8 h; 1, 2, 4, 6, 8, 10, 12 and 14 days), 200 µl of the external release medium was collected for liquid chromatography–tandem mass spectrometry (LC–MS/MS). Immediately after that, the medium was replenished with 200 µl of fresh dissolution medium at 37°C. Samples were collected in triplicate. The exact concentration of FD-TFV was used as a control.

Drug release in vitro through the BBB

HBMVECs and HAs were obtained and prepared for plating of the BBB model. The *in vitro* BBB model was established in a transwell plate as per published protocols [51,52]. HAs were split and seeded on the lower side of 0.4-µm pore size PTFE membrane tissue culture inserts at an initial concentration of 10⁵ cells per well. HBMVECs were incubated for 2 h to allow cells to be saturated on the outside of the insert. After incubation, a confluent layer of HBMVECs was grown on the upper side of the membrane. After 24 h of incubation, the BBB's integrity was measured with transendothelial electrical resistance (TEER) using Millicell ERS microelectrodes (Millipore, MA, USA). Typical TEER values of untreated BBB were observed to be around ~140 Ω/cm². Cells were grown up to 70% confluency, and the predetermined concentration of ND-TFV was introduced into the upper chamber of the transwell insert. Following the introduction to the upper chamber, medium was collected at various time points (30 min; 1 h; 1, 2, 4, 6, 8 and 10 days) from the lower chamber and replenished with fresh medium. Samples were

taken in triplicate for each treatment and stored at -20°C until further analysis by LC–MS/MS. Simultaneously, a separate set up with the same concentration of FD–TFV was used as a control.

Cell uptake & characterization of extended release from NDs

Microglial (HMC3 cells) uptake, retention and release of 1:20 ND–TFV, 1:4 ND–TFV and FD–TFV were determined as per the previously described protocols [53–55]. HMC-3 cells were cultured in 24-well plates at 50,000 cells per well and incubated at 37°C in a humidified 5% CO_2 atmosphere for 24 h to allow for 70% confluency. After 24 h of cell growth, samples were assigned into different treatment groups of 1:20 ND–TFV, 1:4 ND–TFV and FD–TFV and treated at a concentration of 0.0625 mg/ml. Following drug treatment, samples were incubated at 37°C , and cell uptake was determined every hour for 8 h and then at a 24-h time point. For each sample, medium was collected into microcentrifuge tubes and stored at -20°C for later analysis. Samples were taken in triplicate for each treatment. Cells were trypsinized and centrifuged to collect cell pellets, which were washed in 1 ml of PBS and centrifuged at 3000 r.p.m. for 8 min at 4°C . The PBS was then discarded, and cell pellets were resuspended in 200 μl of HPLC-grade methanol, homogenized, and centrifuged at 14,000 r.p.m. for 10 min at 4°C . The methanol extract was then collected into a separate microcentrifuge tube, and the cell debris/pellet was discarded. Samples were then placed into a speed vac at 60°C (Vacufuge Plus, Eppendorf, NY, USA) to dry out. Samples were then stored at -20°C for later analysis and resuspended with 50 μl of PBS for analysis via LC–MS/MS.

In vivo animal care

Healthy BALB/c mice (8 weeks old; 1:1 male:female) were purchased from Charles River Laboratories (CA, USA) and housed under a 12-h/12-h light/dark cycle. A Teklad Certified Global 18% protein rodent diet, (#2018C, Envigo, WI, USA) and water were provided to the mice *ad libitum*. Mice were administered a single intravenous dose. The average weights of phase A and phase B mice were 17.3–18.6 and 17.2–23.4 g, respectively. All procedures were per the current Association for Assessment and Accreditation of Laboratory Animal Care (AAALAC) recommendations. *In vivo* studies were carried out in collaboration with NIH-DAIDS Preclinical Contract Services.

In vivo study

The *in vivo* study was set up into two phases: phase A was performed to determine the maximum tolerated dose (MTD study), and phase B was performed to determine the plasma pharmacokinetics (PK study) of two formulations of TFV (ND and a saline preparation) following an intravenous dose administration.

For the MTD study (phase A), ten males and ten females were divided into five different treatment groups as follows: bicelles only (lipid 5 mg/100 μl); TFV (2 mg/kg) with ND (drug-to-lipid ratio 1:20); TFV (10 mg/kg) with ND (drug-to-lipid ratio 1:7.3); TFV (15 mg/kg) with ND (drug-to-lipid ratio 1:5); and TFV (20 mg/kg) with ND (drug-to-lipid ratio 1:3.8). There were time intervals of 30–45 min between the dose groups, and mice were observed immediately post-dose, 30–45 min post-dose and once daily up to 48 h for toxicity signs. Animals were monitored for any altered clinical signs such as gross motor and behavioral activity and any observable appearance changes.

During the *in vivo* PK study (phase B), three males and three females were divided into two groups. Two-dose formulations of TFV were used in this phase as a single intravenous dose administration; the ND–TFV 20 mg/kg (group 6) and a freshly prepared TFV saline solution at 20 mg/kg (group 7). Additionally, six untreated mice were used to compare as baseline samples. Blood was collected from the retro-orbital sinus of mice under isoflurane anesthesia into tubes containing potassium-EDTA for drug plasma levels at 10 min and 0.5, 1, 3, 8, 24, 48 and 72 h post-dose. Animals were observed immediately post-dose, once daily and before the last blood collection. PK data analysis was performed using the plasma concentrations of TFV via LC–MS/MS.

In vitro & in vivo drug analysis by LC–MS/MS

For *in vitro* drug analysis, TFV was monitored by LC–MS/MS using an AB Sciex (MA, USA) 6500+ QTRAP[®] mass spectrometer coupled to a Shimadzu (MD, USA) Nexera X2 LC system. TFV was measured with the mass spectrometer in positive MRM (multiple reaction monitoring) modes by following the precursor-to-fragment ion transitions 288.1 to 176.2. A Kinetex C8 column (5 μm , 100 \times 4.6 mm) was used for chromatography with the following conditions: buffer A: dH_2O + 0.1% formic acid, buffer B: acetonitrile + 0.1% formic acid; 0–1.0 min 5% B, 1.0–3.0 min gradient to 100% B, 3.0–5.0 min 100% B, 5.0–5.1 min gradient to 5% B, 5.1–6.0 min

5% B. Indinavir (transition 614.6 to 138.9) was used as an internal standard. 50 μ l of the provided sample was mixed with 100 μ l of 50:50 methanol:0.02 N HCl containing 50 ng/ml indinavir as internal standard. Samples were vortexed for 15 s, incubated at room temp for 10 min and centrifuged at $16,100 \times g$ at 4°C in a refrigerated microcentrifuge. LC–MS/MS then evaluated the supernatant. Standard curves were generated using PBS spiked with varying concentrations of TFV or tenofovir disoproxil fumarate (TDF) and processed as described above. The concentration of the drug in each time-point sample was quantified using Analyst 1.7 software (AB Sciex). A value of threefold above the signal obtained from blank PBS was designated the limit of detection. The limit of quantification was defined as the lowest concentration at which back-calculation yielded a concentration within 20% of theoretical and above the limit of detection.

For *in vivo* drug analysis, all reagents used in the plasma samples analysis were either HPLC grade or American Chemical Society reagent grade. CD-1 mouse plasma collected with potassium-EDTA anticoagulant was purchased from BioIVT (NY, USA). The test article TFV (the monohydrate form) was supplied by US Pharmacopeia (MD, USA). Medical Isotopes, Inc. (NH, USA) provided the standard internal TFV-d6, and the purity was assumed to be 100% during stock solution preparation. Calibration standards, quality control samples, blank plasma samples and the study samples were placed into microcentrifuge tubes and all except the blank plasma samples were spiked with an internal standard spiking solution. Samples were briefly vortexed before centrifugation. Following centrifugation, the supernatant was transferred into glass autosampler vials containing Milli-Q water and briefly vortexed. Samples were then stored in a refrigerated autosampler (set at 5°C) before injection into the LC–MS/MS system.

A Phenomenex Synergi Polar-RP column (4 μ m, 100 \times 2 mm) (CA, USA) was used for chromatography with the following conditions: buffer A: 2% acetic acid in water, buffer B: 0.1% acetic acid in acetonitrile; 0–2.0 min 2% B, 2.0–2.01 min gradient to 98% B, 2.01–3.5 min 98% B, 3.51–5 min gradient to 2% B. The concentration of the drug in each time-point sample was quantified using Analyst 1.7 software.

Statistical analysis

Experiments were performed in multiple replicates with data presented as mean \pm standard error of the mean. Each experiment's statistical significance was analyzed using a one-way or two-way analysis of variance with *post hoc* Dunnett's multiple comparisons test by GraphPad Prism (GraphPad, Inc., CA, USA); p-values of ≤ 0.05 were considered significant.

Results

Computational molecular modeling & calculations

There are several challenges in developing long-acting nanoformulations for anti-HIV drugs. In this regard, the current approach to a ND-based formulation has shown significant advancement in the drug delivery approach. The initial characterization with MLSP modeling results for TFV showed lower lipophilic locations surrounding the drug molecule (Figure 1A). The analysis provided the lipophilic potential surrounding each atom or group of atoms and the 3D spatial features of the molecular interactions within the drug molecule. The low lipophilic potential of TFV allows it to be easily entrapped into the bilayer of the ND. The ND is a low-polydispersity, spontaneously forming discoidal shape with a diameter of about ~ 30 nm and a thickness of ~ 5 nm. The ND is composed of long-chain lipids, DPPC, short-chain lipids and DHPC. Additionally, NDs can entrap hydrophobic molecules and have a robust formation and assembly mechanism. The ND represents an attractive drug-delivery model to bypass the BBB to inhibit HIV-1 replication within the brain. Both the MEP and MLSP of TFV were calculated using VEGA-ZZ software; the MEP showed TFV's 3D charge distributions, while MLSP demonstrated the lipophilicity potential of TFV's different regions. Both MEP and MLSP provide insights into the molecule's overall structure, lipophilicity and surface charge of the drug, as well as TFV's interactions with the phospholipids of the bicelle and the way in which it is entrapped. MEP and MLSP are essential tools for understanding the process in which drug-loaded bicelles are self-assembled and encapsulated. As shown in Figure 1A, TFV is an extremely lipophobic molecule (shown in red/orange), limiting its incorporation within the bicellar core. TFV prefers to locate in the external terminals of the phospholipids due to their higher hydrophilicity.

Structural characterization

The size distribution of drug-loaded bicelles was also investigated using dynamic light scattering (DLS). The hydrodynamic radius (R_h) of the NDs was determined using DLS in an aqueous solution to determine the pristine and drug-loaded bicelles' size distribution (Figure 1B). In the pristine bicelles (bicelles without any drug), R_h was approximately 8.5 nm, while the R_h of TFV-NDs was in the range of ~ 10 –13 nm, at which size excess

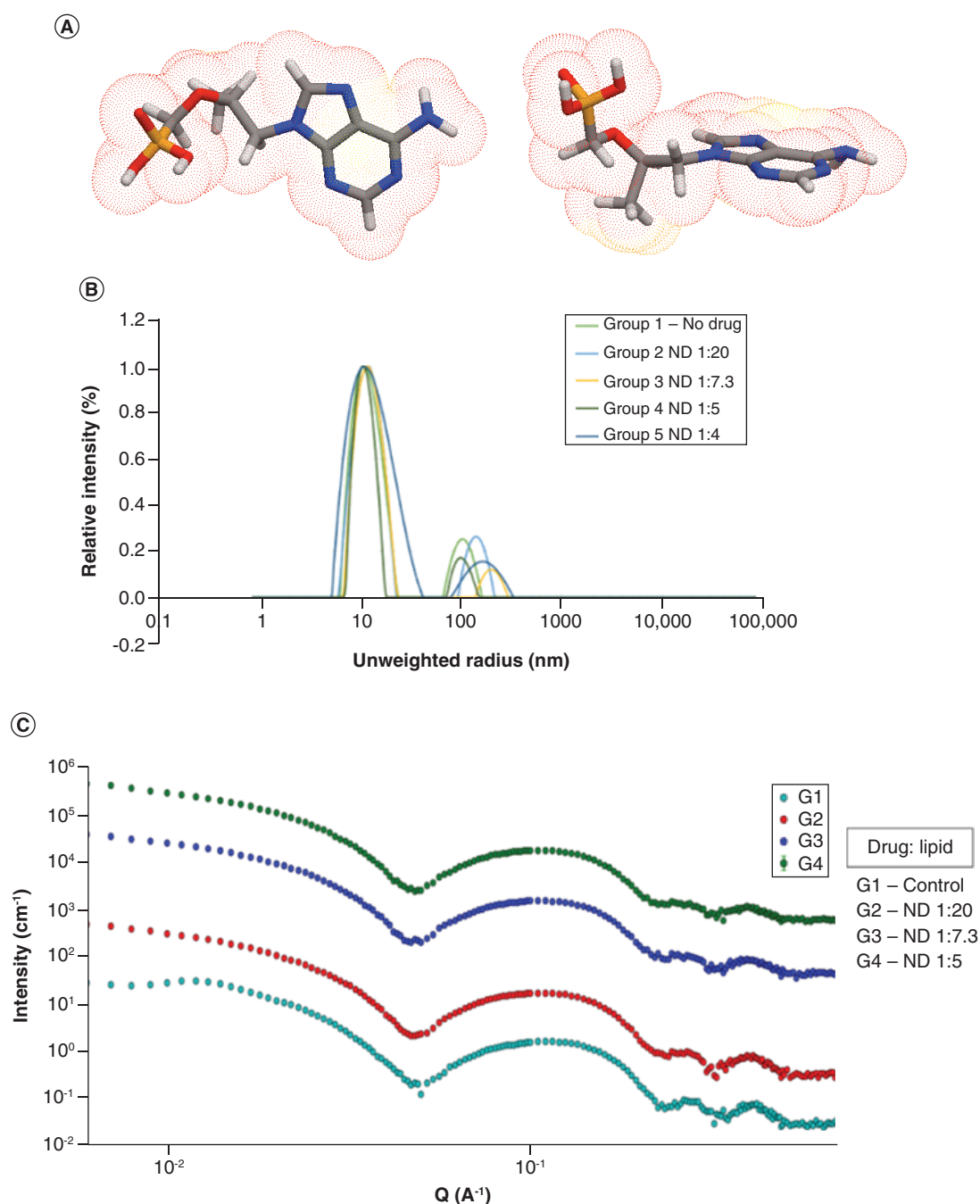


Figure 1. Lipophilicity of Tenofovir and structural characterization of Nanodisc-Tenofovir. (A) Molecular lipophilic surface potential modeling of Tenofovir (TFV), which provided insights into the drug molecule's lipophilicity to help characterize TFV's interactions within the ND. The low lipophilic locations within TFV (red/orange) limit TFV's ability to be incorporated within the ND core. (B) Dynamic light scattering of NDs at varying drug-to-lipid ratios, which was used to determine the size distribution within the solutions. It demonstrated that the hydrodynamic radius of the ND ranged from ~10–13 nm and confirmed the uniformity of the NDs. (C) Small-angle x-ray scattering imaging of NDs at different drug-to-lipid ratios, which was used to determine the discoidal morphology. Retention of the valley and broad bilayer peaks indicated that samples had retained their structures. ND: Nanodisc.

drug molecules precipitate after the NDs' capacity was reached. After drug encapsulation and at lower drug concentrations (drug:lipid ratios of 1:20), a slight increase in size was observed. Further increase in the drug concentrations (drug:lipid ratios of 1:7.3, 1:5 and 1:4) caused the formation of larger bicelles, deformation of the discoidal shape and ultimately the creation of larger aggregations. The DLS results confirmed the uniformity of the NDs for individual TFV-bicelle samples.

SAXS was used to provide the detailed discoidal core-shell architecture of the designed ND with TFV at the different TFV concentrations and drug-to-lipid ratios. As indicated in Figure 1C, the lipid concentrations in TVF-loaded ND formulations were 0.085 wt% in 1:20 ND, 0.031 wt% in 1:7.3 ND, 0.021 wt% in 1:5 ND and 0.017 wt% in 1:4 ND. The TVF concentration was fixed at 0.01 mg/ml in all samples. This technique is sensitive to the electron density distribution in the structure of nanoassemblies averaged over time. The pattern of the X-axis is $1/\text{\AA}$; thus higher X-values correlate to smaller distances. Lipid bilayers within the ND are considered as the lipophilic core, represented in SAXS data as hydrocarbon chains, placed between two shells of hydrophilic phosphatidylcholine head groups. Given that the phosphate group has the highest electron density in the system and is higher than hydrocarbon tails and water, the electron density profile across the bilayer can be approximated as a 'square well'; therefore the SAXS pattern corresponds broadly to the correlation length of head-group distance (Figure 1C). In addition, the slope at the low q region could also determine the lipid aggregates' morphology. SAXS/WAXS can provide insights into the discoidal morphology of the NDs by simulating their electron density profile. SAXS/WAXS probes the average arrangement of molecules in NDs; in a well-defined bicelle, the SAXS data generally contain a series of peaks for $q > 0.07 \text{ \AA}^{-1}$, which correlate to the lipid bilayer structure (Figure 1C). We developed a five-layer core-shell discoidal model in SASView [48,49] to describe the bicellar morphology, as reported in our previous work [14,34,35,47]. Several structural parameters were used within the model, such as the rim thicknesses, trim (t_{rim}), the hydrophilic bilayer shell, $t_{\text{s, norm}}$, crystalline methylene lengths, the terminal methyl of the long-chain phospholipids ($t_{\text{methylene}}$ and t_{methyl}) and radius of the core (R_{core}). Their corresponding electron scattering length densities: ρ_{rim} , $\rho_{\text{s, norm}}$, $\rho_{\text{methylene}}$ and ρ_{methyl} , respectively, and the electron scattering length density of the solvent (water), ρ_{w} , were also considered within the model [47]. The SAXS data of pristine bicelles were the best fit with the five-layer core-shell discoidal model, yielding $t_{\text{s, norm}}$, t_{rim} , disc thickness and R_{core} of 0.5, 2.4, 4.6 and 10.1 nm, respectively; these values were consistent with those reported in the literature [48]. The retention of the valley and broad bilayer peak in SAXS patterns of the ND-TFV indicated that the NDs maintained their structures up to the 1:20 drug-to-lipid ratio. However, the SAXS data indicated the role of TFV's chemical structure and its influence on the bicelles' internal structure. The overall diameter of the bicelles increases with higher drug content, while R_{core} remains practically constant for TFV bicelles. Furthermore, t_{rim} increases abruptly for TFV bicelles with lower drug-to-lipid ratios. This seems consistent with the recent report that the short-chain DHPC with a large spontaneous curvature, mixed with DPPC, induces defects on the DPPC bilayer, thus making the membrane more active in interacting with a foreign hydrophobic species [49]. The R_{core} suggests that TFV mainly resides at the face (closer to the surface and polar water environment) even with increased TFV composition calculated by the constant of R_{core} .

The preliminary characterization of the 1:4 and 1:20 ND formulation established that it was a clear and colorless liquid that can be stored at room temperature (25°C). The molecular characterization indicated that the formulation was a discoidal shape with a hydrodynamic radius of 7.5–13 nm. Overall, based on the drug concentration measured, the majority of the free TFV added in preparation was encapsulated into NDs by the end of the procedure; therefore experiments were designed after measuring the TFV in the initial stock concentration.

Cytotoxicity assay of NDs

To characterize the ND formulation in the biological system in *in vitro* conditions, it was necessary to screen the formulation for cytotoxicity and ensure that it would not induce significant cytotoxicity to microglial (HMC-3) and neuronal (SH-SY5Y) cells. Because our formulation was developed to target the brain, it was essential to observe the effect of ND on these cells for any neurotoxicity or cytotoxicity. A cell viability (MTS) study was performed for empty ND, 1:4 ND-TFV and 1:20 ND-TFV. ND-TFVs were introduced to these cells separately at varying TFV drug concentrations of 0.01–0.1 mg/ml and incubated for 72 h.

Overall, the cell viability results indicated that NDs were less toxic to HMC-3 cells than to SH-SY5Y cells. Additionally, a separate setup to evaluate the effect of empty NDs was conducted, where HMC-3 and SH-SY5Y cells were treated with varying lipid concentrations of the bicellar NDs associated with the TFV concentrations. The results showed that lipid concentrations above 0.08 and 0.05% were significantly cytotoxic for HMC-3 cells

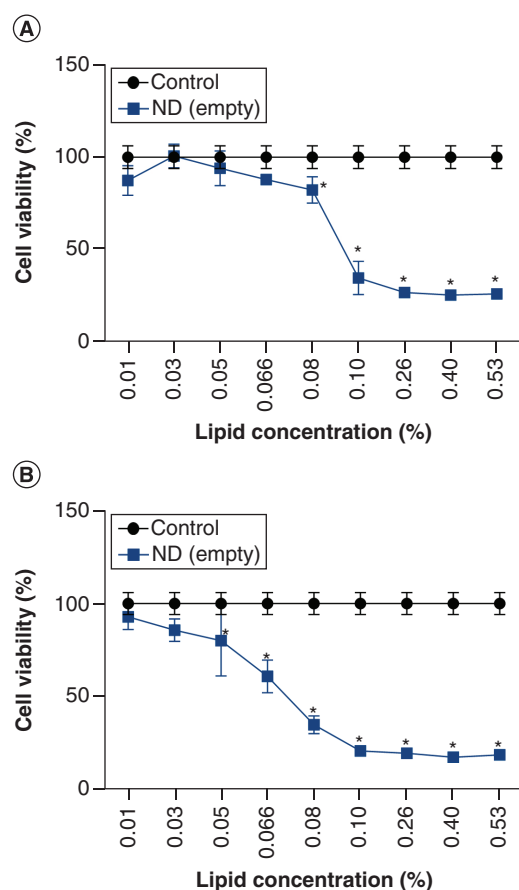


Figure 2. Cell viability assay of nanodiscs (empty) on HMC-3 and SH-SY5Y cells. Cell viability of (A) HMC3 and (B) SY5Y cells with different lipid concentrations (%) of the nanodiscs (0.01–0.53%). Untreated (control) cells were considered to represent 100% viability, and percentage cell survival was monitored based on control. Cell viability percentage was measured as mean \pm standard deviation of three independently replicated experiments. Statistical significance was calculated by one-way analysis of variance with *post hoc* Dunnett's multiple comparisons test.

* $p < 0.05$ was indicative of significance compared with the control.
ND: Nanodisc.

and SH-SY5Y cells, respectively (Figure 2A & B). The 1:20 ND–TFV formulation was found to be significantly toxic at concentrations above 0.0625 mg/ml of TFV for HMC-3 cells (Figure 3A). For SH-SY5Y cells, the effect of 1:20 ND was found only to be statistically significant at 0.1 mg/ml but was observed to decrease cell viability starting at 0.05 mg/ml. The 1:4 ND formulation was significantly toxic at concentrations above 0.05 mg/ml for SH-SY5Y cells (Figure 3B). FD–TFV was not considered to be significantly toxic when compared with the control. This indicated that there was an observed decrease in cell viability at higher drug concentrations associated with higher lipid concentrations.

Effect of empty NDs & ND–TFVs on ROS production by HMC3 & SH-SY5Y cells

While nanomaterials possess unique properties that have increased their use, understanding their interactions within biological systems is important. As a first approach to predicting the inflammatory response of neuronal cells, the ROS production of HMC-3 and SH-SY5Y cells was evaluated. HMC-3 (Figure 4A) and SH-SY5Y cells (Figure 4B) were treated with drug-to-lipid ratios of 1:20 and 1:4 at different TFV drug concentrations (0.01–0.1 mg/ml). A negative control antioxidant (catalase) and positive control (H_2O_2) were used on untreated cells. A simultaneous setup was also performed for empty NDs at varying lipid concentrations. Because a significant drop and then a plateau in cell viability was seen for lipid concentrations above 0.1%, the ROS assay was only done for lipid concentrations of 0.01–0.1% to observe ROS production (Figure 5A & B).

Both HMC-3 cells and SH-SY5Y cells undergoing the treatment of 1:20 NDs were shown to significantly increase ROS production at all the tested concentrations (0.01–0.1 mg/ml) compared with the control (Figure 5A & B). Whereas, both cell lines undergoing the treatment of 1:4 NDs did not show a significant increase in ROS production at tested concentrations up to 0.1 mg/ml. Additionally, we analyzed the FD–TFVs' effect on ROS production of HMC-3 and SH-SY5Y cells. The FD–TFV did not induce a significant increase in ROS production for either cell line, indicating that the FD–TFV does not actively induce ROS production at the tested concentrations. Overall, these results showed that ROS production in 1:4 ND-treated cells was closer to that in untreated cells, suggesting this formulation's potential for further optimization.

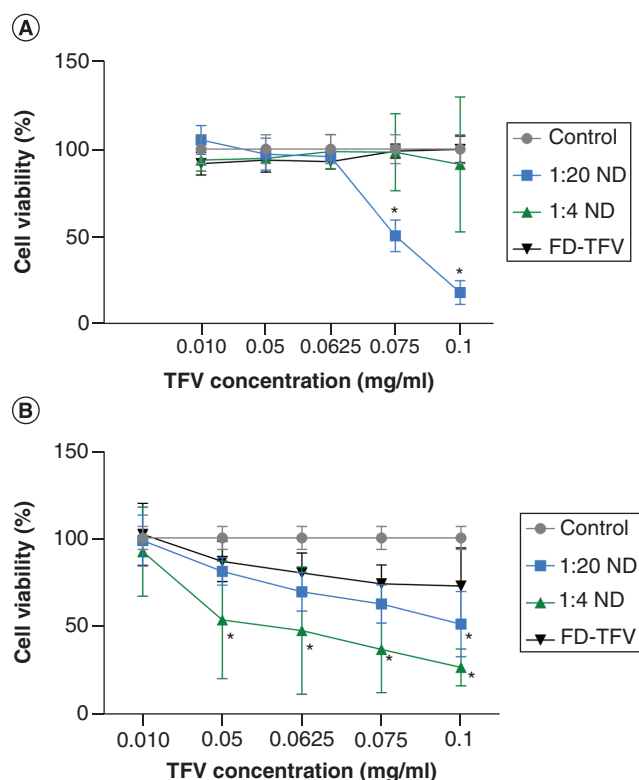


Figure 3. Cell viability assay of tenofovir-loaded nanodiscs on HMC-3 and SH-SY5Y cells. (A) HMC-3 and (B) SH-SY5Y cells were treated with nanodiscs at drug-to-lipid ratios of 1:20 and 1:4, and also with tenofovir free drug. A graphical representation was made of the cell viability percentage at different tenofovir concentrations (0.01–0.1 mg/ml) of the formulations. Untreated (control) cells were considered to represent 100% viability and percentage cell survival was monitored based on control. Cell viability percentage was measured as mean \pm standard deviation of three independently replicated experiments. Statistical significance was calculated by a two-way analysis of variance with *post hoc* Dunnett's multiple comparisons test. * $p < 0.05$ was considered significant compared with the control. FD: Free drug; ND: Nanodisc; TFV: Tenofovir.

In vitro sustained drug-release assay

The NDs' extended drug release characteristic was determined in PBS Tween 20 aqueous solution using an equilibrated dialysis system. The TFV released from the dialysis bag into the outside environment was sampled at different time points up to 14 days and was measured by LC–MS/MS. The dialysis bag used in these experiments was selected for its pore size of 6–8 kDa molecular weight cutoff (MWCO), so that only drug molecules could be transported across the membrane. Simultaneously, a separate setup with the same concentration and volume of FD–TFV was used as a control. Results were expressed as the percentage of total TFV released into the system compared with the initial concentration. It was observed that 63% of FD–TFV was released within 4 h. Compared with FD–TFV, the 1:4 ND–TFV showed 35% drug release within 4 h (Figure 6). Compared with the FD–TFV, the 1:20 ND–TFV showed 0.18% drug release within 4 h and showed a significant, sustained drug release of TFV *in vitro* (Figure 6). Overall, when comparing both 1:20 ND–TFV and 1:4 ND–TFV, the FD–TFV had a significantly faster TFV release, although it is considered delayed in terms of the free drug. However, the 1:20 ND–TFV was shown to have a significantly extended release compared with the 1:4 ND–TFV (Figure 6).

Drug release through the BBB model *in vitro*

The ND was further characterized for its drug-delivery property across the BBB. An *in vitro* BBB model was used to recreate the biological barrier encountered in drug delivery toward HIV-1 residing in the brain and to understand the drug release kinetics of the NDs in the BBB environment. The BBB model's integrity was characterized by measuring the TEER values before and after the ND exposure. The range of TEER values was from 130 to 150 Ω at the beginning and the end of the experiments (Figure 7A). The range of TEER values was similar in all three groups (control, ND–TFV and FD–TFV). The TEER values indicated the consistent integrity of the BBB throughout the experiment, confirming the contribution of the BBB in transporting the ND formulation from the apical to the basolateral side of the BBB. The percentage of drug release of TFV from the 1:4 ND–TFV formulation was compared with that of the FD–TFV, and the pattern indicated that the 1:4 ND–TFV had a sustained release up to 4 days, which was not significantly different from FD–TFV (Figure 7B). Based on the results of this *in vitro* BBB model, 1:4 ND–TFV was observed to have similar drug release characteristics compared with FD–TFV. In contrast, the 1:20 ND–TFV formulation was shown to have extended release properties which were significantly different from those of the FD–TFV. These observations are similar to those seen in the dissolution study (Figure 6).

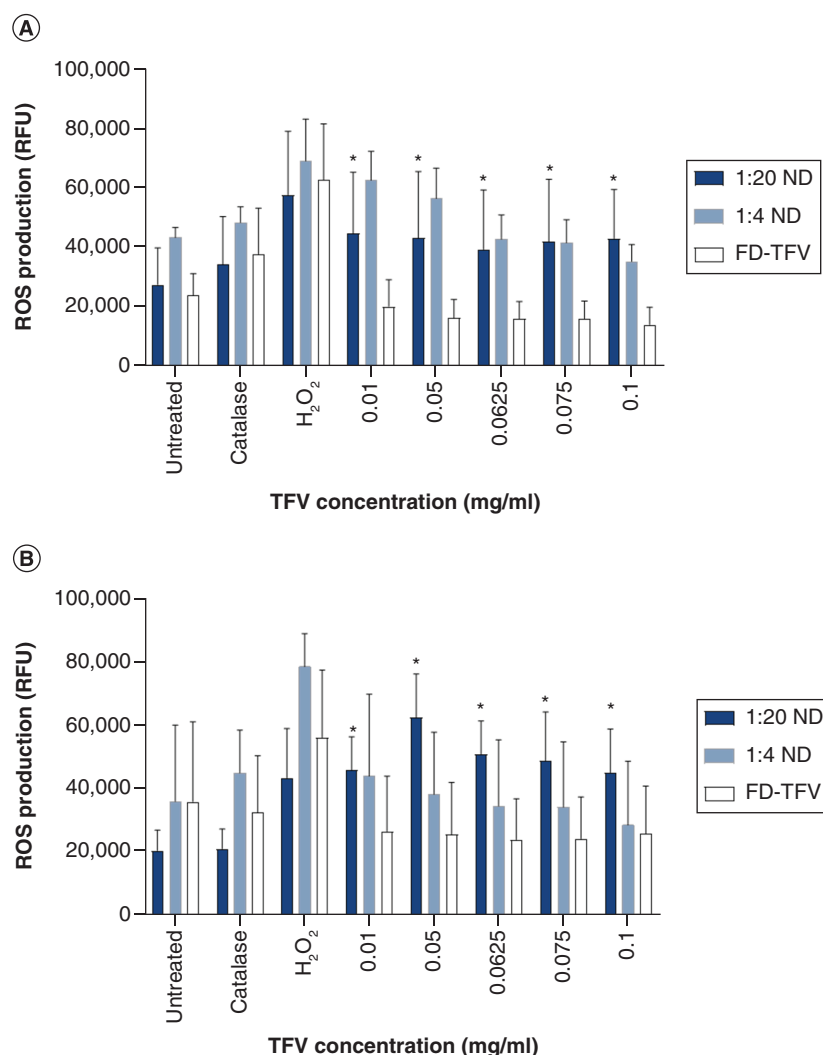


Figure 4. Effect of nanodiscs at 1:20 and 1:4 and free tenofovir on reactive oxygen species production in HMC-3 and SH-SY5Y cells. (A) HMC-3 and (B) SH-SY5Y cells were exposed at different concentrations (0.01–0.1 mg/ml). A graphical representation was made of ROS production; ROS production was measured in terms as mean \pm standard deviation of RFU from three independently replicated experiments. Statistical significance was calculated by two-way analysis of variance with *post hoc* Dunnett's multiple comparisons test.

* $p < 0.05$ was indicative of significance compared with untreated cells.

FD: Free drug; ND: Nanodisc; RFU: Relative fluorescence units; ROS: Reactive oxygen species; TFV: Tenofovir.

Cell uptake & characterization of extended release from ND

To evaluate the intracellular uptake of TFV in microglial cells, an *in vitro* cellular uptake study was performed. The cellular uptake of two formulations (1:4 and 1:20 ND–TFV) and FD–TFV (control) simultaneously monitored the uptake and release of TFV over 24 h. Our results showed different uptake of the two formulations. Maximum uptake was observed at 1 h for 1:20 ND–TFV, at 2 h for 1:4 ND–TFV and at 1 h for FD–TFV (Figure 8). Based on the physiochemical characteristics of TFV (Figure 8), this drug penetration to microglial cells was not very significant. The concentrations measured within the samples were below or around the limit of quantification, indicating that only a small amount of TFV can cross the cell membrane. This small window of cellular uptake could indicate a limited capacity of microglia to uptake TFV, or it could be that the formulation's physical characterization prevents a higher uptake of the NDs. The observed results from this cellular uptake study indicated that 1:4 ND–TFV accumulated TFV within the cell to a greater extent than the 1:20 ND–TFV and FD–TFV formulations. However, the short windows of drug uptake by the microglial cells could indicate that the size and surface charge of the NDs

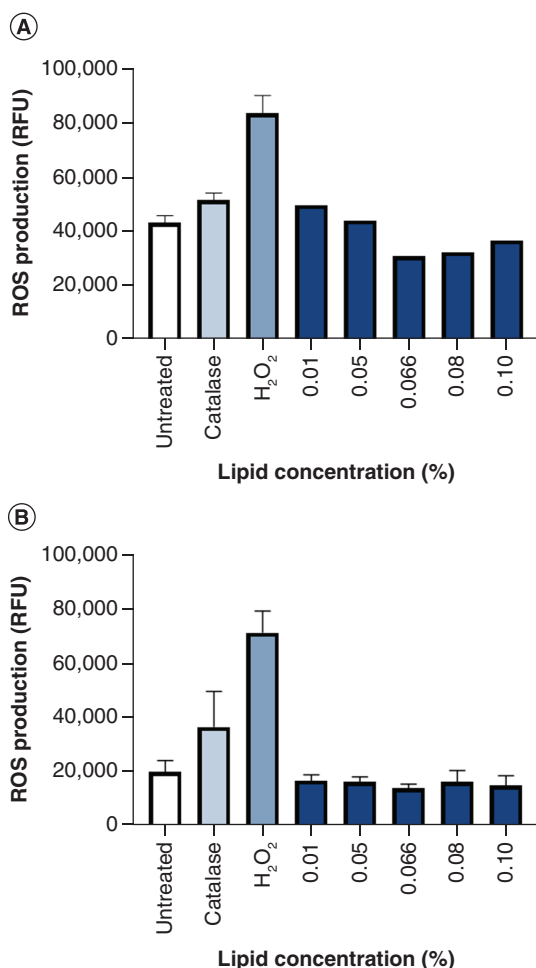


Figure 5. Effect of empty nanodiscs on reactive oxygen species production on HMC-3 and SH-SY5Y cells. (A) HMC-3 and (B) SH-SY5Y cells were exposed at different lipid concentrations (0.01–0.1%). A graphical representation was made of ROS production; ROS production was measured in terms of mean \pm standard deviation of RFU from three independently replicated experiments. Statistical significance was calculated by one-way analysis of variance with *post hoc* Dunnett's multiple comparisons test. RFU: Relative fluorescence units; ROS: Reactive oxygen species.

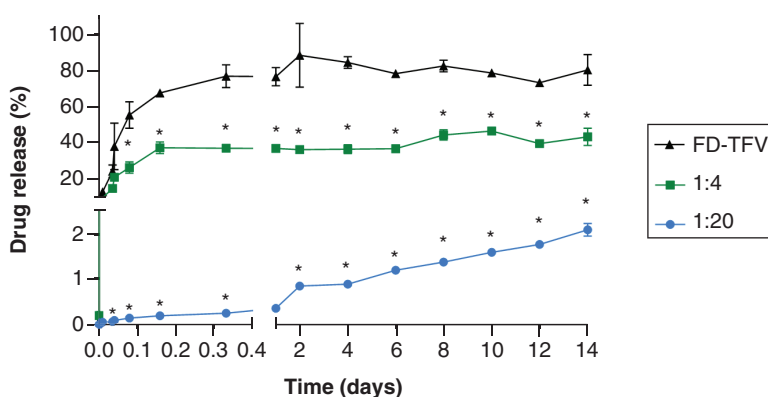


Figure 6. Drug release profiles of nanodiscs (1:20 and 1:4) versus unfornulated tenofovir *in vitro*. Cumulative drug release (%) was measured in terms of mean \pm standard deviation ($n = 3$). Statistical significance was calculated by a two-way analysis of variance with *post hoc* Dunnett's multiple comparisons test. Note: some initial time points are not marked for significance due to overlapping in the graph. * $p < 0.05$ was indicative of significance when compared with unfornulated tenofovir. FD: Free drug; TFV: Tenofovir.

could also be a contributing factor. The overall observation suggested that with the formulation, TFV has a higher chance of getting into the cells compared with FD–TFV.

In vivo MTD study

During the MTD study, male and female BALB/c mice were treated with a single intravenous dose at 0, 2, 10, 15 or 20 mg/kg. Mice were observed at predetermined time points, appeared normal throughout the phase and tolerated the varying ND concentrations well based on the parameters observed. The highest MTD dose level of TFV was selected at 20 mg/kg to continue with further characterization.

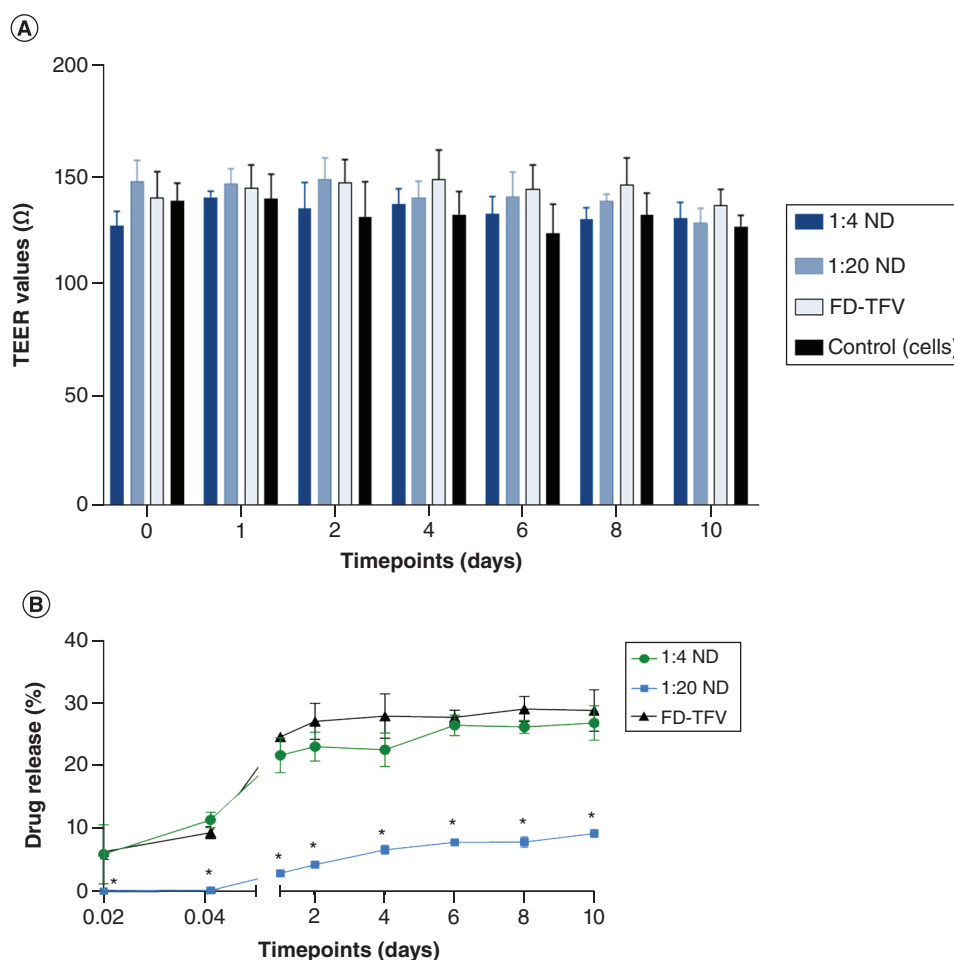


Figure 7. Transendothelial electrical resistance values and sustained drug release from 1:20 and 1:4 nanodiscs in an *in vitro* blood-brain barrier model. 1:20 ND, 1:4 ND and FD-TFV were introduced into the apical chamber of the BBB model. (A) TEER values of the BBB were measured to ensure formulations did not significantly affect the integrity of the BBB. (B) Drug release of formulations through the BBB was observed and measured for up to 10 days. A graphical representation was made in terms of average drug release percentage (%) and was measured in terms of mean % \pm standard deviation ($n = 3$). Statistical significance was calculated by a two-way analysis of variance with *post hoc* Dunnett's multiple comparisons test.

* $p < 0.05$ was indicative of significance when compared with FD-TFV.

BBB: Blood-brain barrier; FD: Free drug; ND: Nanodisc; TEER: Transendothelial electrical resistance; TFV: Tenofovir.

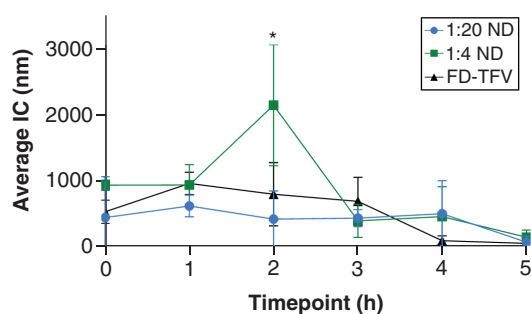


Figure 8. *In vitro* cellular uptake study of nanodiscs (1:4 and 1:20) and unformulated tenofovir. Cellular uptake was measured in terms of average intracellular concentration and was measured in terms of mean \pm standard deviation ($n = 3$). Statistical significance was calculated by a two-way analysis of variance with *post hoc* Dunnett's multiple comparisons test.

* $p < 0.05$ was indicative of significance when compared with FD-TFV.
FD: Free drug; IC: Intracellular concentration; ND: Nanodisc; TFV: Tenofovir.

In vivo PK analysis of NDs

During the PK study, male and female BALB/c mice were administered a single intravenous dose at 20 mg/kg TFV in the ND-TFV formulation (group 6) and FD-TFV in a sterile saline formulation (group 7), and blood

samples were collected for up to 48 and 72 h. The PK data analysis was performed using the plasma concentrations of TFV.

Significant differences in PK parameters were observed between the ND and FD-TFV formulation-administered groups. The initial (C_0) plasma concentrations were $42,387.8 \pm 17,936.2$ and $65,023.1 \pm 43,635.0$ ng for ND-TFV and FD-TFV, respectively. The C_0 in the FD-TFV formulation was almost 1.5-fold that of the ND-TFV formulation. The drug was detected up to 72 h post dosing but was below the lower limit of quantification of the analytical method. The plasma concentration data of up to 24 h was used in calculating the area under the curve (AUC_{0-inf}); AUC_{0-inf} values of 5755.3 ± 1338.2 and 9148.4 ± 4490.9 ng/ml/h were achieved in ND-TFV and FD-TFV, respectively. This followed the trend of C_0 in terms of the magnitude of the differences between the two groups. The AUC_{0-inf} was 1.6-times greater in the FD-TFV formulation compared with ND-TFV. The volume of distribution and the clearance showed a pattern similar to C_0 and AUC_{0-inf} . The volume of distribution measures the relative distribution of the drug in the plasma and extracellular compartments of the body. Given that C_0 was high in the FD-TFV formulation compared with the ND-TFV formulation, it was expected that the volume of distribution would be higher in ND-TFV compared with FD-TFV; the values were 596.9 ± 391.5 and 398.3 ± 179.3 ml/kg for ND-TFV and FD-TFV, respectively. Similar to the volume of distribution, plasma clearance of the drug was faster in ND-TFV compared with FD-TFV; the clearance values were 3694.5 ± 1154.5 and 2528.2 ± 901.8 ml/h/kg in ND-TFV and FD-TFV, respectively. The overall elimination constant (K_{10}) was higher in the ND formulation compared with FD-TNF; this was expected, because C_0 and AUC_{0-inf} were small in the formulation. The K_{10} values were 7.1 ± 1.8 and 6.7 ± 1.1 h⁻¹ in ND-TFV and FD-TFV, respectively.

Discussion

This study focused on the encapsulation of the anti-HIV drug TFV into NDs. Previously NDs have been established as a prominent drug carrier for several anticancer drugs [39]. However, this is the first time the formulation was tested for an anti-HIV drug. Because the ND formulation can encapsulate both hydrophobic and hydrophilic drug molecules, it provides a unique opportunity to expand this work [56]. MEP and MLSP provided information about the surface charge, molecular structure and lipophilicity of TFV and characterized its interactions during entrapment in the ND (Figure 1). MEP and MLSP showed TFV to be an extremely hydrophilic molecule; this can limit the drug's incorporation within the bicellar core, but the ND can entrap both hydrophobic and hydrophilic molecules because of the amphiphilic nature of the phospholipids [30,57]. DLS was used to investigate the size of the drug-loaded-NDs, and the results confirmed the uniformity of the NDs for individual TFV-ND samples (Figure 2). SAXS patterns of the NDs in both 1:4 and 1:20 ND-TFV indicated that the NDs maintained their structures via the retention of the valley and broad bilayer peaks (Figure 1C). However, the SAXS data indicated the role and influence of TFV's chemical structure on the NDs' internal structure. The overall diameter of the NDs increased with higher drug content, and R_{core} remained practically constant for ND-TFVs. The ND formulation was observed to be clear and colorless and miscible with water at room temperature. In addition, an advantage of this formulation was its stability at normal room temperature (25°C).

Cytotoxicity results indicated that the 1:20 ND-TFV formulation caused a decrease in cell viability for HMC-3 and SH-SY5Y cells due to increasing extracellular TFV concentrations (Figure 3), which are associated with higher lipid content (Figure 2 & Supplementary Table 1). While lipid-based formulations are safe and biocompatible and display low toxicity, there is still a level of concern for the high lipid concentrations seen within this study; studies of NDs' toxicity toward neuronal cells remain limited [57]. The results also indicated that SH-SY5Y cells were more susceptible to toxicity than HMC-3 cells, as both ND-TFV formulations (1:4 and 1:20) were observed to cause a decrease in cell viability. Even though the cell viability study was done as per published protocol, it is important to note that it was a direct exposure of cells (HMC3, SH-SY5Y) to ND or free drug in *in vitro* conditions [50]. In clinical settings, most cART drugs are given through oral administration; therefore exposure of brain cells to cART drugs occurs after first-pass metabolism [58]. In this regard, further *in vivo* studies will be performed to evaluate the safety of the ND formulation in the future.

Further evaluation of the ND-TFV on ROS production and oxidative stress showed that 1:20 ND-TFV induced a significant increase in ROS production for both cell lines. In contrast, ROS production in 1:4 ND-TFV-treated cells was closer to that in untreated cells, indicating this formulation's potential for further optimization (Figure 4). The observation of induced ROS production from 1:20 ND-TFV may be due to several factors regarding the ND composition. ROS production on empty ND bicelles was also observed but indicated no significant increase in ROS production (Figure 5). Overall, the optimization of the NDs is dependent on several other factors, such

as their long-term stability, sustained release and therapeutic efficacy. Considering the results from the ROS assay, both 1:20 and 1:4 ND–TFVs were further evaluated to understand the drug release properties of the formulations.

In the drug release study, 1:20 ND–TFV demonstrated a significantly sustained release compared with FD–TFV and 1:4 ND–TFV (Figure 6). It should be noted that during LC–MS/MS analysis of the 1:20 ND's drug release profile, there was a detection of a prodrug-like molecule of TDF, although our formulation was not made with the prodrug TDF. This may be due to by-products or metabolites found from TFV in the 1:20 sample that may have been identified as structurally similar to TDF [59,60]. A loss of TFV into by-products has been previously attributed to pH, which may have been a factor in the 1:20 sample [57]. Additionally, it is essential to note that there was no other detection of the prodrug in the 1:4 ND and FD–TFV samples. The release profile of FD–TFV showed a limitation in the release across the dialysis membrane, which could be attributed to the retardation effect of the tight membrane structure [61]. Considering the structure of the hydrophilic formulation on the surface and the hydrophobic core, the current results agree with the suggestion that the lipid content of a nanostructure helps govern the drug-loading capacity, prolonged release action and overall stability of the formulation, which suggests why 1:20 ND–TFV may have better encapsulation compared with 1:4 ND–TFV [62]. In addition, because the formulation has an automatic encapsulation property without any experimental procedure, the amount of the drug it will hold also largely depends on how well the ND is formed with a concentration of lipids [36,62]. Overall, the drug release study established that 1:20 ND–TFV was significantly more stable than 1:4 ND–TFV, which could translate into better pharmacokinetics *in vivo*.

The drug release study through an *in vitro* BBB model showed the 1:20 ND formulation to have extended release properties that were significantly different from those of the FD–TFV, whereas the 1:4 ND–TFV had similar drug release properties to FD–TFV (Figure 7B). It is noteworthy that the drug release of the FD–TFV and ND–TFV across the BBB is regulated by the biological transporters present on both sides of the BBB [63]. Often it was observed that the drug release capacity across the BBB might be higher; however, those formulations struggle with sustained-release properties, as indicated in our observation. While FD–TFV and 1:4 ND–TFV could cross the BBB efficiently, they did not have a sustained release property like that of the 1:20 ND–TFV formulation. It is also worth noting that these formulations did not compromise the integrity of the BBB (Figure 7A). These formulations were also evaluated for their microglial uptake via an *in vitro* cell uptake study. As microglia are considered the major reservoir of HIV-1, observation of their drug uptake would help determine the brain's drug retention capacity. The results showed a maximum TFV uptake observed at 1 h for 1:20 ND, 1 h for FD–TFV and 2 h for 1:4 ND–TFV (Figure 8). The 2 h of drug uptake by the microglial cells could indicate that the size, surface charge and PEGylation of the NDs could be contributing factors [64,65].

Based on our *in vitro* studies, an *in vivo* optimization study was also designed to observe the MTD and PK of 1:4 and 1:20 ND–TFVs in mice. In this regard, it is important to mention that both male and female BALB/c mice used for this study were 8 weeks old, selected considering the clinical relevance of the study: the majority of people with HIV-1 are living longer and aging with the virus due to the wide availability of cART in recent years [66]. This opens up the opportunity to optimize the NDs and current cART drugs in an older animal model. However, we acknowledge the fact that older mice may be more susceptible to tenofovir toxicity compared with younger mice [67]. The MTD study indicated that out of several doses tested in the mice, the highest dose was well tolerated without any adverse clinical observation, based on any visible symptoms. An *in vivo* PK analysis was performed on the measurable plasma concentration of TFV after administration in two different intravenous formulations: an ND–TFV formulation and FD–TFV. The plasma concentration–time profile and PK parameters showed significant differences between the two formulations. Higher C_0 and AUC_{0-inf} were obtained in the FD–TFV formulation compared with the ND–TFV formulation. This suggested that a significant part of the ND formulation had been distributed to the extracellular compartment of the body and penetrated intracellularly, because nanoparticles are known to have higher penetration/permeation, possibly including brain tissues and other organs [63]. However, tissue distribution studies are needed to confirm this observation. TFV is known to have poor permeation/penetration across the cell. However, once inside the cells, TFV converts to a diphosphate form that stays inside the cell for a long time due to its charged nature [68,69]. Administering TFV as the ND formulation may improve therapeutic outcomes in HIV-1 infection. Furthermore, the volume of distribution and clearance values also suggested higher extravascular distribution of ND–TFV compared with FD–TFV. However, differences in C_0 , AUC_{0-inf} , volume of distribution and clearance parameters of the two groups (ND–TFV and FD–TFV) were not statistically significant ($p > 0.05$) due to high standard deviation. This high standard deviation was due to the smaller size of the animals used in the study and could be decreased by increasing the group size. We intend

to perform comprehensive PK, tissue distribution and pharmacodynamic studies in a big group to determine the statistical significance between the two formulations.

Both *in vitro* and *in vivo* characterization studies indicate that further optimization of the formulation is needed to obtain more significant PK information. The structural lipid composition of the NDs was changed to some extent to be more closely aligned with a liposomal structure. The change in structure provided more stability in holding TFV within its aqueous core and indicated extended drug release properties. A similar types of structures have been well documented to have sustained release properties because of their amphiphilic nature [70]. However, the present study could not provide anti-HIV-1 efficacy of either formulation against HIV-1, which is an important aspect of the optimization of this nanodrug. Considering the importance of the drug-to-lipid ratio in both the 1:4 and the 1:20 formulations, the study mainly focused on the cytotoxicity, sustainability, pharmacokinetics and drug release properties of these formulations *in vitro* and *in vivo*. Given that the present study has established the above-mentioned characteristics of these formulations, further research will be needed to check the therapeutic efficacy of these formulations *in vitro* and *in vivo*. ND formulations are well characterized in cancer therapy, which provides us the confidence to take these formulations for further characterization [33,35,39].

The use of this formulation for anti-HIV drugs and the effect of cART drug-to-lipid ratio on their pharmacological properties are reported for the first time in this study, which is completely different than anything we have established in the past. Therefore the clinical relevance of the current observations is significant, because this ND formulation can hold a clinically relevant level of hydrophobic and hydrophilic cART drugs and cross the BBB. This observation further indicates that these formulations can be potential candidates for next-generation anti-HIV drug delivery with further optimization. Overall, the study established that NDs could provide drug stability and sustained drug release properties to the TFV formulation. This is the first time an ND formulation has been characterized for antiretroviral drug delivery to the brain and its potential for anti-HIV treatment.

Conclusion

Overall, this study's results contribute to developing an ND-based delivery toward the brain to treat HIV-1. However, as observed, an increase in the ND's lipid content, as seen in the 1:20 formulation, could affect the cellular environment when using higher concentrations. The greater lipid content within the 1:20 formulation allows it to have more stability than the 1:4 formulation, enabling it to have a sustained drug release for a more extended period. In the meantime, the 1:4 formulation is shown to have minimal cytotoxicity on neuronal cells but has a relatively faster drug release according to the *in vitro* and *in vivo* studies. The ND formulation offers an attractive solution for the treatment of active and slowly replicating HIV-1 in the brain. This is a significant observation, as controlling the slowly replicating HIV from HIV reservoir organs such as the brain will provide a significant improvement in treatment outcomes for HAND.

Executive summary

- The study for the first time demonstrated the utilization of a nanodisc (ND) formulation for anti-HIV drug delivery across the human blood–brain barrier in *in vitro* conditions.
- The ND formulation allows an unbiased investigation of the interaction between the drug and the cells, keeping other physicochemical characteristics invariant.
- The self-assembling capacity of NDs provides an opportunity to encapsulate both hydrophobic and hydrophilic combination antiretroviral therapy drugs and develop a sustained release of the drug formulation; this formulation can host a complete set of drugs in one molecular structure.
- The efficacy of targeted delivery across the blood–brain barrier makes the formulation unique for future delivery of therapeutics.
- The study established an important role of the drug-to-lipid ratio in the ND formulation which is important for further success of this nanodrug *in vitro* and *in vivo*.

Supplementary data

To view the supplementary data that accompany this paper please visit the journal website at: www.futuremedicine.com/doi/suppl/10.2217/nnm-2022-0043

Acknowledgments

The authors acknowledge SRI International for the detailed animal study. The Preclinical Pharmacology Core facility at UT Southwestern Medical Center is acknowledged for LC–MS/MS analysis of *in vitro* studies.

Financial & competing interests disclosure

This work was supported by research support in part with federal funds from the National Institute of Allergy and Infectious Diseases, National Institutes of Health, Department of Health and Human Services, under contract no. HHSN272201400006I and NIH grants #1R15NS108815-01 and #1R01AI147731-01A1. Additionally, internal funding was provided by the University of Texas Rio Grande Valley. A US patent application has been filed on this work (PCT/US21/46708). The authors have no other relevant affiliations or financial involvement with any organization or entity with a financial interest in or financial conflict with the subject matter or materials discussed in the manuscript apart from those disclosed. This manuscript will be submitted to NIHMS for further circulation.

No writing assistance was utilized in the production of this manuscript.

Ethical conduct of research

The authors have obtained appropriate institutional protocols for all *in vitro* studies. All animal studies were conducted in collaboration with NIAIDS and SRI International as per their institutional protocols. The study data was analyzed by SRI International and reanalyzed by the authors.

The authors state that they have obtained appropriate institutional review board approval or have followed the principles outlined in the Declaration of Helsinki for all human or animal experimental investigations.

Open access

This work is licensed under the Attribution-NonCommercial-NoDerivatives 4.0 Unported License. To view a copy of this license, visit <http://creativecommons.org/licenses/by-nc-nd/4.0/>

References

Papers of special note have been highlighted as: • of interest; •• of considerable interest

1. Barré-Sinoussi F, Ross AL, Delfraissy JF. Past, present and future: 30 years of HIV research. *Nat. Rev. Microbiol.* 11(12), 877–883 (2013).
2. Rao KS, Ghorpade A, Labhasetwar V. Targeting anti-HIV drugs to the CNS. *Expert Opin. Drug Deliv.* 6(8), 771–784 (2009).
3. UNAIDS. 90-90-90: an ambitious treatment target to help end the AIDS epidemic (2014). www.unaids.org/sites/default/files/media_asset/90-90-90_en.pdf
4. UNAIDS. Ending AIDS: progress towards the 90-90-90 targets (2017). www.unaids.org/en/resources/documents/2017/20170720_Global_AIDS_update_2017
5. Lanman T, Letendre S, Ma Q, Bang A, Ellis R. CNS neurotoxicity of antiretrovirals. *J. Neuroimmune Pharmacol.* 16(1), 130–143 (2021).
6. Ghosh AK, Sarkar A, Mitsuya H. HIV-associated neurocognitive disorder (HAND) and the prospect of brain-penetrating protease inhibitors for antiretroviral treatment. *Med. Res. Arch.* 5(4), 1113 (2017).
7. Patra JK, Das G, Fraceto LF, Campos EVR *et al.* Nano based drug delivery systems: recent developments and future prospects. *J. Nanobiotechnology* 16(1), 71 (2018).
8. Gerson T, Makarov E, Senanayake TH, Gorantla S, Poluektova LY, Vinogradov SV. Nano-NRTIs demonstrate low neurotoxicity and high antiviral activity against HIV infection in the brain. *Nanomed. Nanotechnol. Biol. Med.* 10(1), 177–185 (2014).
9. Wang Y, Miao L, Satterlee A, Huang L. Delivery of oligonucleotides with lipid nanoparticles. *Adv. Drug Deliv. Rev.* 87, 68–80 (2015).
10. Torchilin VP. Recent advances with liposomes as pharmaceutical carriers. *Nat. Rev. Drug Discov.* 4(2), 145–160 (2005).
11. Dreher MR, Liu W, Michelich CR, Dewhirst MW, Yuan F, Chilkoti A. Tumor vascular permeability, accumulation, and penetration of macromolecular drug carriers. *J. Natl Cancer Inst.* 98(5), 335–344 (2006).
12. Hsu HJ, Bugno J, Lee SR, Hong S. Dendrimer-based nanocarriers: a versatile platform for drug delivery. *Wiley Interdiscip. Rev. Nanomed. Nanobiotechnol.* 9(1). doi:10.1002/wnan.1409 (2017).
13. Lai SM, Chiou YC, Chen GF, Liao MY, Tzen JT, Lai PS. Enhanced nuclear localization of photosensitizer using artificial oil bodies for photodynamic therapy. *Smart Sci.* 4(4), 167–172 (2016).
14. Patri AK, Majoros IJ, Baker JR. Dendritic polymer macromolecular carriers for drug delivery. *Curr. Opin. Chem. Biol.* 6(4), 466–471 (2002).
15. Ashley CE, Carnes EC, Phillips GK *et al.* The targeted delivery of multicomponent cargos to cancer cells by nanoporous particle-supported lipid bilayers. *Nat. Mater.* 10(5), 389 (2011).
16. Liu M, Huang G, Cong Y, Tong G, Lin Z, Yin Y, Zhang C. The preparation and characterization of micelles from poly (γ -glutamic acid)-graft-poly (L-lactide) and the cellular uptake thereof. *J. Mater. Sci. Mater. Med.* 26(5), 1–9 (2015).
17. Blanco E, Shen H, Ferrari M. Principles of nanoparticle design for overcoming biological barriers to drug delivery. *Nat. Biotechnol.* 33(9), 941–951 (2015).

18. Agarwal R, Singh V, Journey P, Shi L, Sreenivasan SV, Roy K. Mammalian cells preferentially internalize hydrogel nanodiscs over nanorods and use shape-specific uptake mechanisms. *Proc. Natl Acad. Sci. USA* 110(43), 17247–17252 (2013).
19. Chithrani BD, Ghazani AA, Chan WC. Determining the size and shape dependence of gold nanoparticle uptake into mammalian cells. *Nano Lett.* 6(4), 662–668 (2006).
20. Truong NP, Whittaker MR, Mak CW, Davis TP. The importance of nanoparticle shape in cancer drug delivery. *Expert Opin. Drug Deliv.* 12(1), 129–142 (2015).
21. Nagahama K, Kawano D, Oyama N, Takemoto A, Kumano T, Kawakami J. Self-assembling polymer micelle/clay nanodisk/doxorubicin hybrid injectable gels for safe and efficient focal treatment of cancer. *Biomacromolecules* 16(3), 880–889 (2015).
22. Singh AT, Ghosh M, Forte TM, Ryan RO, Gordon LI. Curcumin nanodisk-induced apoptosis in mantle cell lymphoma. *Leuk. Lymphoma* 52(8), 1537–1543 (2011).
23. Sun W, Parowatkin M, Steffen W, Butt HJ, Mailänder V, Wu S. Ruthenium-containing block copolymer assemblies: red-light-responsive metallopolymers with tunable nanostructures for enhanced cellular uptake and anticancer phototherapy. *Adv. Healthc. Mater.* 5(4), 467–473 (2016).
24. Sun W, Wen Y, Thiramanas R *et al.* Red-light-controlled release of drug–Ru complex conjugates from metallopolymer micelles for phototherapy in hypoxic tumor environments. *Adv. Funct. Mater.* 28(39), 1804227 (2018).
25. Ernsting MJ, Murakami M, Roy A, Li SD. Factors controlling the pharmacokinetics, biodistribution and intratumoral penetration of nanoparticles. *J. Control. Release* 172(3), 782–794 (2013).
26. Kong G, Braun RD, Dewhirst MW. Hyperthermia enables tumor-specific nanoparticle delivery: effect of particle size. *Cancer Res.* 60(16), 4440–4445 (2000).
27. Tan J, Shah S, Thomas A, Daniel Ou-Yang H, Liu Y. The influence of size, shape and vessel geometry on nanoparticle distribution. *Microfluid. Nanofluidics* 14(1–2), 77–87 (2013).
28. Gratton SE, Ropp PA, Pohlhaus PD *et al.* The effect of particle design on cellular internalization pathways. *Proc. Natl Acad. Sci. USA* 105(33), 11613–11618 (2008).
29. Qiu Y, Liu Y, Wang L, Xu L *et al.* Surface chemistry and aspect ratio mediated cellular uptake of Au nanorods. *Biomaterials* 31(30), 7606–7619 (2010).
30. Bozzuto G, Molinari A. Liposomes as nanomedical devices. *Int. J. Nanomed.* 10, 975 (2015).
31. Xing H, Hwang K, Lu Y. Recent developments of liposomes as nanocarriers for theranostic applications. *Theranostics* 6(9), 1336 (2016).
32. Sharma A, Madhunapantula SV, Robertson GP. Toxicological considerations when creating nanoparticle-based drugs and drug delivery systems. *Expert Opin. Drug Metab. Toxicol.* 8(1), 47–69 (2012).
33. Iqbal U, Albaghdadi H, Nieh MP *et al.* Small unilamellar vesicles: a platform technology for molecular imaging of brain tumors. *Nanotechnology* 22(19), 195102 (2011).
34. Nieh MP, Kucerka N, Katsaras J. Spontaneously formed unilamellar vesicles. *Methods Enzymol.* 465, 3–20 (2009).
35. Aresh W, Liu Y, Sine J, Thayer D *et al.* The morphology of self-assembled lipid-based nanoparticles affects their uptake by cancer cells. *J. Biomed. Nanotechnol.* 12(10), 1852–1863 (2016).
- **Nanodisc (ND)-based drug delivery enhances uptake of cancer drugs by cancer cells.**
36. Liu Y, Xia Y, Rad AT, Aresh W, Nieh MP. Stable discoidal bicelles: a platform of lipid nanocarriers for cellular delivery. *Methods Protoc.* 1522, 273–282 (2017).
- **The ND platform can be used for cellular delivery of drugs.**
37. Nieh MP, Dolinar P, Kucerka N *et al.* Formation of kinetically trapped nanoscopic unilamellar vesicles from metastable nanodiscs. *Langmuir* 27(23), 14308–14316 (2011).
- **NDs can provide a stable structure to encapsulate a large amount of drug molecules.**
38. Nieh MP, Raghunathan VA, Kline SR *et al.* Spontaneously formed unilamellar vesicles with path-dependent size distribution. *Langmuir* 21(15), 6656–6661 (2005).
- **Spontaneous formation of NDs provides self-encapsulating capacity of drug.**
39. Rad AT, Chen CW, Aresh W, Xia Y, Lai PS, Nieh MP. Combinational effects of active targeting, shape, and enhanced permeability and retention for cancer theranostic nanocarriers. *ACS Appl. Mater. Interfaces* 11(11), 10505–10519 (2019).
- **NDs encapsulating cancer drug have enhanced permeability to cancer cells.**
40. World Health Organization. Consolidated guidelines on the use of antiretroviral drugs for treating and preventing HIV infection: recommendations for a public health approach. (2016).
41. Liu Y, Li M, Yang Y, Xia Y, Nieh MP. The effects of temperature, salinity, concentration and PEGylated lipid on the spontaneous nanostructures of bicellar mixtures. *Biochim. Biophys. Acta* 1838(7), 1871–1880 (2014).
- **The high lipid concentration in NDs stabilizes them and prevents the formation of multilamellar vesicles.**

42. Rad AT, Hargrove D, Daneshmandi L, Ramsdell A, Lu X, Nieh MP. Codelivery of paclitaxel and parthenolide in discoidal bicelles for a synergistic anticancer effect: structure matters. *Adv. NanoBiomed. Res.* 2(1), 2100080 (2022).
43. Rad AT, Malik S, Yang L, Oberoi-Khanuja TK, Nieh MP, Bahal R. A universal discoidal nanoplatform for the intracellular delivery of PNAs. *Nanoscale* 11(26), 12517–12529 (2019).
44. Rad AT, Bao Y, Jang HS *et al.* Aggregation-enhanced photoluminescence and photoacoustics of atomically precise gold nanoclusters in lipid nanodiscs (NANO2). *Adv. Funct. Mater.* 31(10), 2009750 (2021).
45. Laad P, Shete G, Modi SR, Bansal AK. Differential surface properties of commercial crystalline telmisartan samples. *Eur. J. Pharm. Sci.* 49(2), 109–116 (2013).
46. Testa B, Carrupt PA, Gaillard P, Billois F, Weber P. Lipophilicity in molecular modeling. *Pharm. Res.* 13(3), 335–343 (1996).
47. Zhao N, Francis NL, Calvelli HR, Moghe PV. Microglia-targeting nanotherapeutics for neurodegenerative diseases. *APL Bioeng.* 4(3), 030902 (2020).
48. DiFabio J, Chodankar S, Pjerov S *et al.* The life science x-ray scattering beamline at NSLS-II. *AIP Conference Proceedings*. AIP Publishing LLC, NY USA, 030049 (2016).
49. Yang L. Using an in-vacuum CCD detector for simultaneous small-and wide-angle scattering at beamline X9. *J. Synchrotron. Radiat.* 20(2), 211–218 (2013).
50. Roy U, Drozd V, Durygin A *et al.* Characterization of nanodiamond-based anti-HIV drug delivery to the brain. *Sci. Rep.* 8(1), 1603 (2018).
- **Anti-HIV drug can be reformulated as a nanodrug for targeted delivery to the brain.**
51. Roy U, Rodríguez J, Barber P, das Neves J, Sarmento B, Nair M. The potential of HIV-1 nanotherapeutics: from *in vitro* studies to clinical trials. *Nanomedicine* 10(24), 3597–3609 (2015).
- **HIV nanotherapy is a potential option to reduce the side effects of current HIV medicine.**
52. Roy U, Bulot C, zu Bentrup KH, Mondal D. Specific increase in MDR1 mediated drug-efflux in human brain endothelial cells following co-exposure to HIV-1 and saquinavir. *PLoS ONE* 8(10), e75374 (2013).
53. Gendelman HE, Balkundi S, Nowacek AS *et al.* Comparative manufacture and cell-based delivery of antiretroviral nanoformulations. *Int. J. Nanomedicine* 6, 3393 (2011).
54. Nowacek AS, Miller RL, McMillan J *et al.* NanoART synthesis, characterization, uptake, release and toxicology for human monocyte-macrophage drug delivery. *Nanomedicine* 4(8), 903–917 (2009).
55. Roy U, Ding H, Pilakka-Kanthikeel S *et al.* Preparation and characterization of anti-HIV nanodrug targeted to microfold cell of gut-associated lymphoid tissue. *Int. J. Nanomedicine* 10, 5819–5835 (2015).
56. Shao J, Kraft JC, Li B *et al.* Nanodrug formulations to enhance HIV drug exposure in lymphoid tissues and cells: clinical significance and potential impact on treatment and eradication of HIV/AIDS. *Nanomedicine* 11(5), 545–564 (2016).
57. Zhang W, Sun J, He Z. The application of open disk-like structures as model membrane and drug carriers. *Asian. J. Pharm. Sci.* 8(3), 143–150 (2013).
58. Masters MC, Landay AL, Robbins PD *et al.* Chronic HIV infection and aging: application of a geroscience-guided approach. *J. Acquir. Immune Defic. Syndr.* 89(Suppl. 1), S34–S46 (2022).
59. Golla VM, Kurmi M, Shaik K, Singh S. Stability behaviour of antiretroviral drugs and their combinations. 4: characterization of degradation products of tenofovir alafenamide fumarate and comparison of its degradation and stability behaviour with tenofovir disoproxil fumarate. *J. Pharm. Biomed. Anal.* 131, 146–155 (2016).
60. Li L, Johnson LM, Krovi SA, Demkovich ZR, van der Straten A. Performance and stability of tenofovir alafenamide formulations within subcutaneous biodegradable implants for HIV pre-exposure prophylaxis (PrEP). *Pharmaceutics* 12(11), 1057 (2020).
61. Hua S. Comparison of *in vitro* dialysis release methods of loperamide-encapsulated liposomal gel for topical drug delivery. *Int. J. Nanomedicine* 9, 735 (2014).
62. Chauhan I, Yasir M, Verma M, Singh AP. Nanostructured lipid carriers: a groundbreaking approach for transdermal drug delivery. *Adv. Pharm. Bull.* 10(2), 150–165 (2020).
63. Grabrucker AM, Ruozzi B, Belletti D *et al.* Nanoparticle transport across the blood brain barrier. *Tissue Barriers* 4(1), e1153568 (2016).
64. Foroozandeh P, Aziz AA. Insight into cellular uptake and intracellular trafficking of nanoparticles. *Nanoscale Res. Lett.* 13(1), 339 (2018).
65. Zhang F, Lin YA, Kannan S, Kannan RM. Targeting specific cells in the brain with nanomedicines for CNS therapies. *J. Control. Release* 240, 212–226 (2016).
66. Jang E, Lee JK, Inn KS, Chung EK, Lee KT, Lee JH. Renal dysfunction and tubulopathy induced by high-dose tenofovir disoproxil fumarate in C57BL/6 Mice. *Healthcare (Basel)* 8(4), 417 (2020).
67. Zhang Z, Lu Y, Qi J, Wu W. An update on oral drug delivery via intestinal lymphatic transport. *Acta Pharm. Sin. B* 11(8), 2449–2468 (2021).

68. Spinks CB, Zidan AS, Khan MA, Habib MJ, Faustino PJ. Pharmaceutical characterization of novel tenofovir liposomal formulations for enhanced oral drug delivery: *in vitro* pharmaceutics and Caco-2 permeability investigations. *Clin. Pharmacol.* 9, 29–38 (2017).
69. Brooks KM, Ibrahim ME, Castillo-Mancilla JR *et al.* Pharmacokinetics of tenofovir monoester and association with intracellular tenofovir diphosphate following single-dose tenofovir disoproxil fumarate. *J. Antimicrob. Chemother.* 74(8), 2352–2359 (2019).
70. Karumanchi DK, Skrypai Y, Thomas A, Gaillard ER. Rational design of liposomes for sustained release drug delivery of bevacizumab to treat ocular angiogenesis. *J. Drug Deliv. Sci. Technol.* 47, 275–282 (2018).